THE JOURNAL OF BIOLOGICAL CHEMISTRY VOL. 281, NO. 26, pp. 18193–18200, June 30, 2006


# Crystal Structure of the Herpes Simplex Virus 1 DNA Polymerase*

Received for publication, March 15, 2006, and in revised form, April 24, 2006 Published, JBC Papers in Press, April 24, 2006, DOI 10.1074/jbc.M602414200

**Shenping Liu[1], John D. Knafels, Jeanne S. Chang, Gregory A. Waszak, Eric T. Baldwin[2], Martin R. Deibel, Jr.[3], Darrell R. Thomsen[4], Fred L. Homa[5], Peter A. Wells, Monica C. Tory, Roger A. Poorman[6], Hua Gao, Xiayang Qiu, and Andrew P. Seddon**

*From Pfizer Inc., Groton, Connecticut 06340*

**Herpesviruses are the second leading cause of human viral diseases. Herpes Simplex Virus types 1 and 2 and Varicella-zoster virus produce neurotropic infections such as cutaneous and genital herpes, chickenpox, and shingles. Infections of a lymphotropic nature are caused by cytomegalovirus, HSV-6, HSV-7, and Epstein-Barr virus producing lymphoma, carcinoma, and congenital abnormalities. Yet another series of serious health problems are posed by infections in immunocompromised individuals. Common therapies for herpes viral infections employ nucleoside analogs, such as Acyclovir, and target the viral DNA polymerase, essential for viral DNA replication. Although clinically useful, this class of drugs exhibits a narrow antiviral spectrum, and resistance to these agents is an emerging problem for disease management. A better understanding of herpes virus replication will help the development of new safe and effective broad spectrum anti-herpetic drugs that fill an unmet need. Here, we present the first crystal structure of a herpesvirus polymerase, the Herpes Simplex Virus type 1 DNA polymerase, at 2.7 Å resolution. The structural similarity of this polymerase to other α polymerases has allowed us to construct high confidence models of a replication complex of the polymerase and of Acyclovir as a DNA chain terminator. We propose a novel inhibition mechanism in which a representative of a series of non-nucleosidic viral polymerase inhibitors, the 4-oxo-dihydroquinolines, binds at the polymerase active site interacting non-covalently with both the polymerase and the DNA duplex.**

Only eight distinct viruses, spanning three subfamilies, designated α, β, and γ, of the greater than 80-member Herpesviridae family are known to cause clinically significant diseases in humans (1). Herpesviruses possess a common replication cycle in which the viral polymerase (POL)[7] functions at multiple points and is thus an attractive target for the development of antiherpetic drugs (1–3). In fact, Acyclovir, the first selective anti-viral drug developed, targets the viral polymerase as a nucleotide analog (2). However, drug resistances against these nucleotide analog drugs are severe, especially among the immunocompromised population (4, 5). Alternative approaches, such as non-nucleotide drugs, may be needed (1, 6).

The *Herpesvirus* polymerases exhibit a 34–90% primary sequence identity and range in size from 1012 to 1242 amino acids. Herpes Simplex 1 DNA polymerase (HSV POL), the prototype for the herpesvirus POL family, has 1,235 amino acid residues and exhibits all the enzymatic functions of a polymerase (7). In addition to a polymerase activity required to extend the DNA primer chains, HSV POL possesses an intrinsic 3′-5′-exonuclease activity that serves as a proofreading activity to ensure the high fidelity of DNA replication (8). HSV POL has also been reported to have an intrinsic RNase H activity that presumably functions in the removal of RNA primers during the processing of Okazaki fragments (9). The RNase H activity was initially attributed to a 5′-3′-exonuclease function associated with HSV POL; however, this activity was subsequently attributed to the potent 3′-5′-exonuclease of HSV POL (7). *In vivo*, the extreme COOH terminus of the cognate polymerase has been shown at the molecular level to interact with an accessory factor, UL42, that serves to increase the processivity of the polymerase (10, 11). During the predominant rolling circle mode of DNA replication, HSV POL forms a large complex with the viral primase·helicase complex (7), the details of which, at a molecular level, have yet to be elucidated. Based on sequence similarity, HSV POL belongs to the POL α family, which includes human polymerase α and polymerases from animals and other viruses. Crystal structures of POL α from thermophilic and archaebacteria and the apo, editing, and replication complexes of the bacteriophage RB69 POL have been reported (12–16). These structures not only revealed the general architecture of the POL α polymerase but also provide important information on interactions of the enzyme with DNA and nucleotides.

Detailed analysis of the HSV POL structure presented here with reference to those previously reported polymerase structures provides valuable insight into the domain functions, conformational changes required for catalysis, and an enhanced understanding of the herpesvirus DNA replication. Further, combined with other experimental data, this analysis enabled us to propose models for the dead-end complex formed with Acyclovir and of a prototype compound of non-nucleotide POL inhibitors, 4-oxo-dihydroquinolines (4-oxo-DHQ).

## EXPERIMENTAL PROCEDURES

*Protein Expression and Purification*—A fusion protein consisting of bacterial maltose-binding protein and full-length HSV 1 POL was constructed with either one factor *X*a cleavage site at the linker region or with a second factor *X*a site right after Asn-42 of HSV POL. The maltose-binding protein-HSV POL fusion protein was expressed in a bacu-

* The costs of publication of this article were defrayed in part by the payment of page charges. This article must therefore be hereby marked "*advertisement*" in accordance with 18 U.S.C. Section 1734 solely to indicate this fact.

*The atomic coordinates and structure factors (code 2GV9) have been deposited in the Protein Data Bank, Research Collaboratory for Structural Bioinformatics, Rutgers University, New Brunswick, NJ (http://www.rcsb.org/).*

[1] To whom correspondence should be addressed: Pfizer Inc., Exploratory Medicinal Sciences, Eastern Point Rd., Groton, CT 06340. Tel.: 860-686-6959; Fax: 860-686-2095; E-mail: shenping.liu@pfizer.com.

[2] Present address: Pharmaceutical Research Inst., Bristol-Myers Squibb Co., Rte. 206 and Provinceline Rd., Princeton, NJ 08540.

[3] Present address: Proteos, 4717 Campus Dr., Kalamazoo, MI 49008.

[4] Present Address: 6916 Willson Dr., Kalamazoo, MI 49009.

[5] Present address: University of Pittsburgh, Dept. of Molecular Genetics and Biochemistry, School of Medicine, 200 Lothrop St., BSTWR W1256, Pittsburgh, PA 15261.

[6] Present address: PharmOptima LLC, 4717 Campus Dr., Kalamazoo, MI 49008.

[7] The abbreviations used are: POL, DNA polymerase; HSV, Herpesvirus; HSV POL, herpes simplex 1 DNA polymerase; DHQ, dihydroquinolines; CHAPS, 3-[(3-cholamidopropyl)dimethylammonio]-1-propanesulfonic acid.

**TABLE 1**

**Data collection, phasing, and refinement statistics**

Numbers in parentheses are in the highest resolution shell. Wavelengths used were 1.0 Å 0.9794 Å, 0.9504 Å for native and derivative crystals, respectively. Resolutions observed and used were 111.0-2.7 Å for native and 50-3.2 Å for derivative (3.5 Å for phasing). The native data set was collected on a crystal soaked in 1 mM mercury acetate for 2 h. Four weakly bound mercury atoms are found in the structure. The derivative $I(hkl)$ and $I(-h-k-l)$ were separated for scaling. R.m.s.d., root mean square deviation.

| Crystal | Native | SeMet+$(CH_3)_3PbOOCCH_3$ | |
|---|---|---|---|
| **Unit cell** | 103.917, 125.550, 220.577 | 105.073, 123.887, 217.564 | |
| **No. unique reflections** | 82,195 | 91,186 | 90,713 |
| **No. total measurements** | 2,103,907 | 2,050,368 | 1,028,698 |
| **Completeness** | 100 (100) | 99.8 (99.9) | 99.7 (98.7) |
| **$I/s$** | 30.2 (2.4) | 28.2 (5.4) | 17.9 (3.1) |
| **$R_{merge}$ (%)** | 7.1 (84.9) | 7.0 (34.3) | 7.8 (42.9) |
| **Redundancy** | 9.5 (8.2) | 9.2 (8.3) | 5.1 (4.6) |
| **Phasing** | | | |
| Number of sites | | 37 SeMet, 14 Pb | |
| $R_{cullis}$ | | 0.91 (0.95) | |
| $R_{cullis\ anom}$ | | 0.77 (0.92) | 0.78 (0.94) |
| **Phasing power acentric** | | 0.74 (0.61) | |
| Centric | | 0.61 (0.24) | |
| **Refinement** | | | |
| $R_{work}$ (%) | 23.5 | | |
| $R_{free}$ (%) | 29.8 | | |
| **R.m.s.d. from ideal geometry** | | | |
| Bond length | 0.017 | | |
| Bond angles | 1.70° | | |

lovirus/insect cell system, and cells were harvested 65 h post-infection by slow speed centrifugation. Proteins were resolved by phosphocellulose chromatography, and the pooled fusion protein was cleaved by treatment with endogenous protease (one factor *X*a site construct) or by factor *X*a (construct with two factor *X*a sites). The cleaved product, Asn-42-COOH-terminal, was further purified on a hydroxyapatite column followed by a heparin column. The purified protein was >95% pure as shown via SDS-PAGE and characterized by mass spectrum analysis, amino acid analysis, and $NH_2$-terminal analysis. The purified polymerase proved to be highly active with radioactive nucleotide incorporation assay. Selenomethionine-labeled HSV POL was expressed in the baculovirus insect cell system (17). Judged by the disappearance of normal methionine, ~60% of normal methionine was substituted with selenomethionine.

*Crystallization and Data Collection*—Purified protein was concentrated to ~20 mg/ml in a buffer of 20 mM HEPES, pH 7.0, 100 mM guanidine HCl, 5 mM dithiothreitol, 11.1% $Me_2SO$, and 10% glycerol. Crystals were grown by hanging drop vapor diffusion against a well buffer of 100 mM HEPES, pH 7.0, 50 mM ammonium sulfate, 5 mM dithiothreitol, 100 mM guanidine HCl, and 4% polyethylene glycol-3350. For cryoprotection, crystals were transferred into a cryoprotectant buffer of 100 mM HEPES, pH 7.0, 60 mM ammonium sulfate, 5 mM dithiothreitol, 100 mM guanidine HCl, 10% polyethylene glycol-3350, 11% $Me_2SO$, 10% polyethylene glycol-1000 by slow exchange with mother liquor and soaked in this buffer overnight. For heavy atom soaking, heavy atom compounds were added into cryoprotectant buffer to desired concentrations. Crystals were mounted with cryoloops and cooled immediately into liquid nitrogen afterward. The crystals of HSV POL belong to space group $P2_12_12_1$, with typical unit cell dimensions of a = 103.9 Å, b = 125.6 Å, c = 220.6 Å. The diffraction data were collected on beamline 17ID of Advanced Ploton Source at Argonne National Laboratory (Argonne, IL) and processed with the program HKL2000 (18). Further data processing was conducted using program suite CCP4 (19) (Table 1).

*Structure Determination and Refinement*—Molecular packing suggested two molecules/asymmetric unit. Molecular replacement attempts with RB69 POL as search model failed to give solutions. Soaking of many different heavy atom compound solutions either destroyed the diffraction or introduced very few specific binding sites, thus very little phase information. The severe non-isomorphism between different crystals also severely limits the usage of multiple isomorphous replacement phasing method. The most promising heavy atom derivative was from crystals soaked in 20 mM trimethyllead acetate overnight: useful anomalous signal could be detected in a two-wavelength data set up to 5.0 Å. At this resolution the model building was impossible despite some secondary structure elements from one of the 3′-5′-exonuclease domains, and one of the palm subdomains could be recognized. The structure of HSV POL was eventually determined using multiple anomalous dispersion method with a crystal formed by selenomethionine-incorporated protein and soaked in 20 mM trimethyllead acetate overnight. The wavelengths were chosen at the absorption edges of selenium and lead, respectively, to maximize the anomalous and dispersive signals (Table 1). Heavy atom sites were found with the program SHELXD (20). Because selenomethionine incorporation in insect cells is still not very robust (17), the incorporation level of the protein used in crystallization is ~50–60%. Of a total of 40 selenomethionine sites 37 were found, along with 14 lead sites. Heavy atom refinement and phase calculations were carried out using the program MLPHARE implemented in CCP4 (19). The maximum useful phase information is at 3.5 Å. After heavy atom refinement and phase calculations, initial electron density was improved with the program SOLOMON (21), and the quality of the electron density was ready for tracing. A phased rotation and translation search of fragments of known POL structures of the POL $\alpha$ family in the experimentally phased electron density map was used to locate some known domains with the program MOLREP (22). Selenomethionine sites were used for sequence registration. A model was built with the program O (23). After model building, the initial model was refined against higher resolution native data (Table 1) with the refinement programs CNX (24) and REFMAC (25). In the final model, molecule A starts at 60 and ends at 1197, with peptides 504–513, 640–700, 1036–1066, and 1080–1135 missing. Molecule B starts at 59 and ends at 1197, with peptides 236–240, 641–700, and 1098–1135 missing. Pep-

tide 641–700 is the linking peptide between the $NH_2$-terminal domain and the polymerase domain. Peptide 1198 to the carboxyl end of the molecule (1235) is involved in accessory factor binding (10, 11). Other missing peptides are all located at the protein surface. Some surface peptides such as NB, NC, P3, P4, and PB (Fig. 1) have very large temperature factors, reflecting their flexibility. To compare protein structures, domain superimposition of HSV POL with other polymerase structures was carried out using the program LSQMAN (26).

*4-Oxo-DHQ Binding Assay*—Mixtures of HSV POL (100 nM) and/or activated calf thymus DNA (Amersham Biosciences) and/or a $^{14}$C-labeled 4-oxo-DHQ (PHA-708620, an analog of PNU-183792) (6) were incubated for 5 min and then subjected to rapid filtration by centrifugation (3 min, 14,000 × *g*) in a Microcon centrifugal concentrator unit (30,000 MWCO, cellulose membrane; Millipore). Aliquots of the resulting filtrate were scintillation counted (Ultima Gold scintillant). Comparison of the quantity of the 4-oxo-DHQ in the filtrate of test samples relative to control samples ([$^{14}$C]4-oxo-DHQ only) yielded a measure of the amount of bound and free 4-oxo-DHQ. All steps were performed at ambient temperature. The buffer solutions used were either 6.4 mM sodium HEPES, 1 mM Tris-HCl, 11.7 mM KCl, 0.025 mM NaCl, 4.5 or 10 mM $MgCl_2$ (or $CaCl_2$), 0.1 mM EDTA, 2 mM CHAPS, 4.5 mM dithiothreitol, 5% glycerol, 5% $Me_2SO$, 0.046 mg/ml of bovine serum albumin, 0.001% azide, pH 7.5.

## RESULTS

The overall architecture of HSV POL closely resembles that of other POL α structures despite being at least 300 amino acid residues longer and exhibiting a low sequence homology (range 16–50%). HSV POL is comprised of 6 structure domains: a pre-$NH_2$ domain, an $NH_2$ domain, a 3′-5′-exonuclease domain, and polymerase palm, fingers, and thumb domains. Based on sequence conservation in the POL α polymerases family (5), the exonuclease domain contains conserved regions exo I, exo II (region IV), and exo III (δ-C region). Regions III and VI belong to the fingers, regions I, II, and VII are located in the palm subdomain, and the thumb subdomain contains the conserved region V (Fig. 1*A*). These domains assemble to form a disk-like shape around a central hole, with the $NH_2$ and COOH termini at opposite sides of the protein (Fig. 1*A*). Three grooves can be seen emanating from the central hole (Fig. 1*B*). The first groove, located at the interface of $NH_2$-terminal and exonuclease domains, is lined with positively charged side chains (Fig. 1*B*). In the RB69 POL replicating complex structure (14, 15), the analogous groove binds the 5′-extension of the single-stranded DNA template (16). In HSV POL these positively charged side chains are predicted to interact with the phosphate backbone of the single-stranded DNA template. The second groove, located between the exonuclease domain and the tip of the thumb domain, leads to the putative exonuclease active site. In the RB69 POL editing complex structures (14, 15), the unwound primer strand binds in this groove. The DNA duplex, in both the editing and replicating complex structures, binds to a third groove formed by the palm and thumb subdomains (15, 16).

In the HSV POL crystal form there are two molecules in the crystallographic asymmetry unit. Each molecule adopts a slightly different conformation and can be superimposed as two groups. Group 1 consists of the pre-$NH_2$-terminal, $NH_2$-terminal, the exonuclease domain, and the finger domain (root mean square deviation 0.8 A for 595 Cα). Group 2 consists of the palm and thumb domains (root mean square deviation 0.95 A for 300 Cα). Both conformations are close to the open state observed in the apo RB69 POL structure (14); however, some conformational differences are observed when either of the two conformations of the HSV POL molecules is compared with RB69 POL and other POL α structures. No consistent concerted motions among different domains are observed when multiple structures are compared. The 3′-5′-exonuclease domain and polymerase palm, fingers, and thumb domains of HSV POL can be individually superimposed with the equivalent domain structures from other POL α structures. In the POL α-conserved regions all the residues of HSV POL can be superimposed with those in RB69 POL. For example, the residues of the secondary structures of the 3′-5′-exonuclease domain, essential for the fidelity of the viral DNA duplication (27), can be overlaid with those of RB69 POL, bringing Asp-368, Glu-370, and Asp-471 of HSV POL to Asp-114, Glu-116, and Asp-222 of RB69 POL that form the metal binding site for the nuclease activity (15). Key residues for polymerase catalysis are located on the palm and fingers domains and are superimposable with those of other POL α and will be discussed in the modeling section. In the structures of RB69 POL the thumb domain interacts with the backbone of DNA duplex, and the tip and base of this domain adopt different conformations at the editing and replication modes. Interestingly, the conformation of the thumb domain of HSV POL is similar to that of the replicating conformation of RB69 POL and thus does not require a large conformational change upon DNA binding (Fig. 1*B*). Sequence conservation in the thumb domain does not need to be high, as DNA duplex binding involves collective interactions; however, high sequence conservation of this domain in the herpes POL family as well as the conserved region V across POL α family does make sense in the context of interacting with DNA duplex backbone (*e.g.* Arg-959, Arg-1039, His-1051, and Arg-1071). Large deletions or insertions in these domains of the POL α family usually occur at loops or form some additional secondary structures distant from the catalytic centers.

HSV POL possesses a 250-amino acid $NH_2$-terminal extension relative to RB69 POL that forms the pre-$NH_2$- and part of the $NH_2$-terminal domains. The pre-$NH_2$-terminal domain is unique to the herpes DNA POL family, and its function is unknown. With the exception of the first 42 residues, which are not present in our construct and are unique to herpes simplex 1 and 2 POL, the sequence similarities of this domain are high among the herpes POL family members. With the exception of two short β strands forming an anti-parallel β sheet, this domain lacks defined secondary structural elements (Fig. 2*A*) and interacts mainly with the 3′-5′-exonuclease domain located at the surface of the protein. Topologically, the highly conserved FYNPYL sequence at the $NH_2$ terminus of this domain is positioned directly upstream of the putative binding groove for the 5′-extension of the single-stranded DNA template (Fig. 2*A*), suggesting a possible role for this domain in interacting with the viral primase·helicase complex during leading strand DNA synthesis (7). If confirmed, disruption of these interactions would provide a new path to design anti-herpes drugs.

The $NH_2$-terminal domain of HSV POL consists of three motifs. The first motif (141–200 and 299–362) consists of two almost perpendicular β3 sheets (N1, N9 and N11, and N2, N3, N4, N10) plus short α helices NA and NE. The second motif (201–298) is a βαββαβ fold (N5, NC, N6, N7, ND, and N8), and the third (594–639) consists of two helixes separated in primary sequence from the first two motifs by the 3′-5′-exonuclease domain (Fig. 2*B*). The first motif is conserved within the herpes POL family, but with the $NH_2$-terminal extension it is much larger than the equivalent domain in known α POL structures. The βαββαβ motif is a typical RNA binding motif (RNP) found in ribonucleoproteins (28). The four β strands and two α helices of this motif approximately superimpose with those of human ribonucleoprotein A1 (PDB code 1HA1) with a root mean square deviation of 1.61 for 46 Cα atoms. In the RNP motif, the face of the β sheet above the α helices provides an open platform for RNA binding (28). The analogous face in HSV POL con-

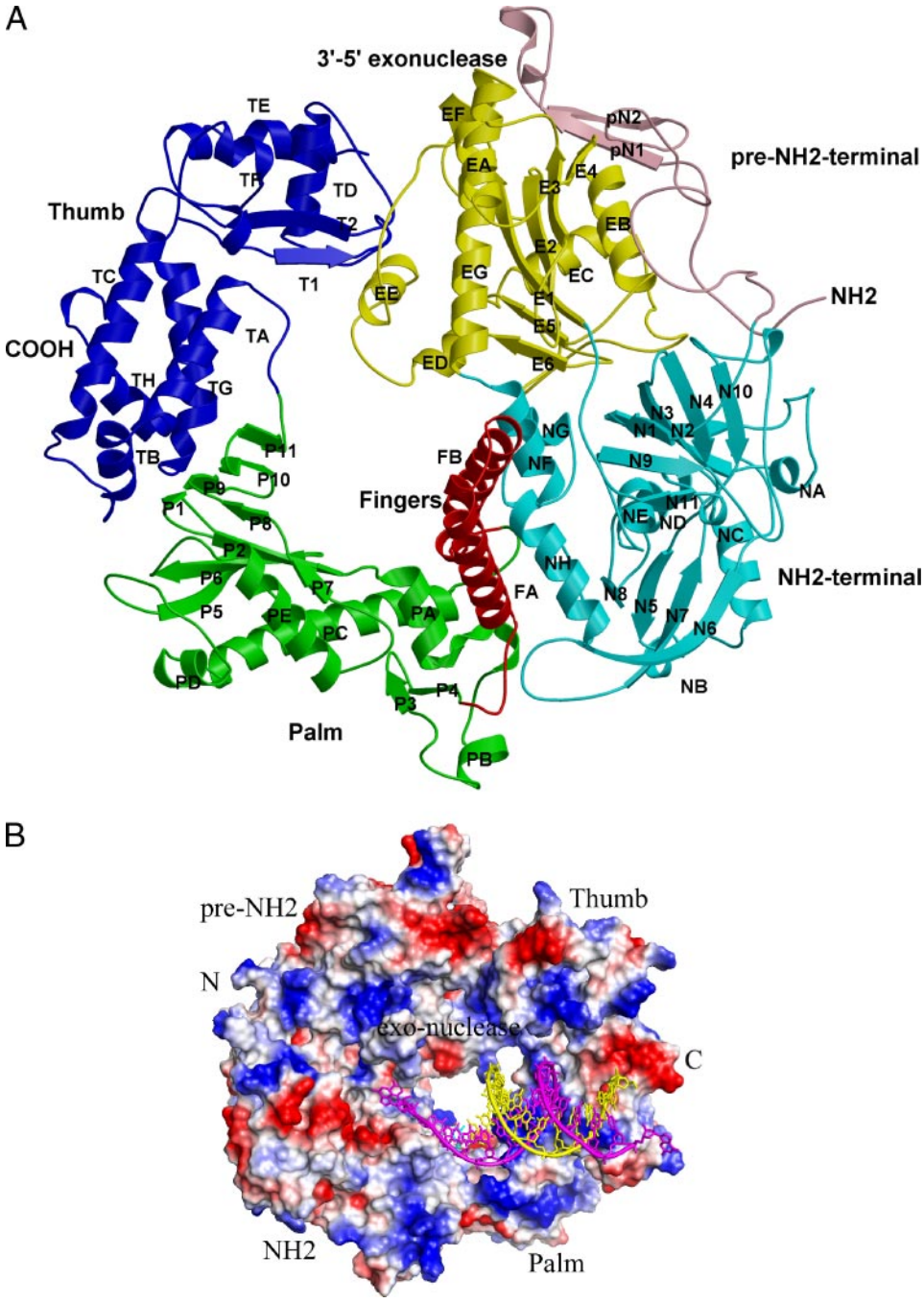


FIGURE 1. *A*, overall structure of herpes simplex 1 DNA polymerase in ribbon diagram. Pre-$NH_2$ domain, $NH_2$-terminal domain, 3′-5′-exonuclease domain, polymerase palm subdomain, finger subdomain, and thumb subdomain are colored *pink*, *cyan*, *yellow*, *green*, *red*, and *blue*, respectively. Domain boundary of HSV POL: *pre-$NH_2$-terminal domain*, from $NH_2$-terminal to 140; *$NH_2$-terminal domain*, 141–362 and 594–639; *3′-5′-exonuclease domain*, 363–593; *palm domain*, 701–766 and 826–956; *fingers domain*, 767–825; and *thumb domain*, 957–1197. The COOH-terminal accessory protein binding peptide, 1200–1235, is missing in both molecules. Secondary structure assignments: *pre-$NH_2$ domain*, pN1, 74–79; pN2, 94–99. *$NH_2$-terminal domain*, N1, 146–149; N2, 151–157; NA, 169–173; N3, 179–187; N4, 193–198; N5, 204–208; NB, 209–212; NC, 221–232; N6, 249–257; N7, 266–272; ND, 276–283; N8, 290–293; NE, 299–305; N9, 314–318; N10, 341–345; N11, 350–352; NF, 594–604; NG, 610–615; NH, 618–632. *3′-5′-exonuclease domain*, E1, 363–372; E2, 390–399; E3, 408–414; EA, 421–429; E4, 436–440; EB, 443–456; E5, 464–464; EC, 471–480; E6, 521–524; ED, 525–530; EE, 540–547; EF, 560–566; EG, 568–592. *Palm subdomain*, P1, 707–709; P2, 713–718; PA, 721–730; PB, 740–745; P3, 755–757; P4, 761–764; PC, 831–855; PD, 859–865; P5, 879–885; P6, 889–895; PE, 902–917; P7, 924–926; P8, 928–930; P9, 932–935; P10, 940–945; P11, 950–953. *Fingers*, FA, 773–794; FB, 797–814 and 817–822. *Thumb subdomain*, TA, 964–979; TB, 981–989; TC, 1005–1022; T1, 1033–1036; TD, 1050–1060; T2, 1071–1072; TE, 1087–1095; TF, 1146–1151; TG, 1158–1176; TH, 1181–1191. *B*, an electrostatic representation of HSV POL DNA binding surface, with duplicating DNA strands superimposed from RB69 POL structure. *Red* and *blue* colors represent negative and positive charges, respectively. Modeled template DNA strand in *magenta* and primer strand in *yellow*, with *ribbon diagram* for the backbone and *stick model* for bases and riboses. The incoming nucleotide is also modeled to indicate the polymerase active site (carbon atoms in *cyan*). *Panel B* is roughly a back view of *panel A*. Figs. 1*A* and 3, *A*, *B*, and *D*, are generated with the program MOLSCRIPT (32) and Figs. 1*B* and 2, *A* and *B*, with PyMol (33).

tains a cluster of highly conserved positive charged (Arg-255, Arg-270, and Arg-302) and aromatic (Tyr-204, Tyr-206, and Tyr-293) residues that could interact with the RNA backbone and bases (Fig. 2*B*). The third motif of this domain has a structure common to others members of the POL α family and consists of two α helices of similar length, NF and NH, connected by a short α helix NG (HSV POL) or a loop. Together with the first and the third motifs of this domain, the putative RNA binding face forms a cleft that would likely accommodate the binding of an RNA or DNA terminus. In support of this, all of the RB69 POL structures contain a guanine nucleotide in this pocket (14–16).

Of a controversial nature are reports that HSV POL possesses an intrinsic 5′-3′-RNase H activity that specifically degrades RNA·DNA heteroduplexes or duplex DNA (7, 9). This activity is required for the excision of the RNA primers that initiate the synthesis of Okazaki fragments at the replication fork during the lagging strand DNA synthesis (7). The existence of an RNA binding motif in this domain suggests that this could be the 5′-3′-RNase H catalytic center. Inspection of the HSV POL structure reveals a cluster of residues that could form a metal ion binding site necessary for nuclease activity. In the RB69 POL structures a cluster of highly conserved residues, Glu-294, Asp-306, and Tyr-204, are observed near the phosphate tail of the guanine nucleotide. Topologically, binding of a single strand RNA primer or DNA in this cleft during DNA replication is plausible when one considers that the cleft is on the opposite side of the DNA binding surface (Fig. 1, *A* and *B*). Conversely, by analogy with other POL α, the possibility cannot be excluded of the involvement of this domain in the autoregulation of the POL synthesis via binding to its own mRNA (12, 13).

A model of the replication complex of HSV POL was constructed by

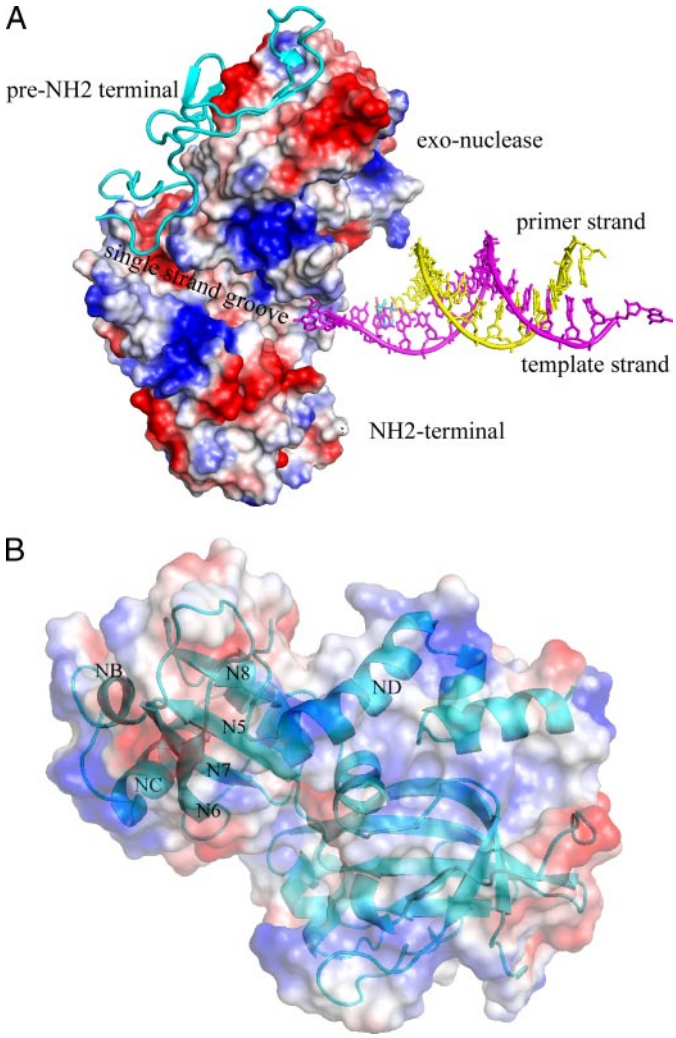


FIGURE 2. **Unique functional domains of herpes simplex 1 DNA polymerase.** *A*, a *ribbon diagram* of the pre-$NH_2$-terminal domain in *cyan*, with electrostatic surface representation of the putative single-stranded DNA binding groove. For clarity, only surfaces from $NH_2$-terminal and exonuclease domains are shown. The DNA duplex is modeled. *B*, *ribbon diagram* of the $NH_2$-terminal domain embedded in the electrostatic surface representation to show the putative RNA binding cleft. The $\beta\alpha\beta\beta\alpha$ motif is on the *left*.

superimposing individual domains of HSV POL onto those of the replication complex of RB69 POL. The palm domain of the replicating RB69 POL complex was chosen as the reference, and the HSV POL domains were individually superimposed onto the RB69 POL structure. In all apo-POL $\alpha$, as well as in the editing complex RB69 POL structures, there is a kink at the highly conserved residues Asn-815-Ser-816 on the second $\alpha$ helix (FB) of the finger domain. In the replicating RB69 POL complex structure the FB helix is continuous, and our model was adjusted accordingly. The continuous nature of helix FB is required to bring the highly conserved Tyr-818-Gly-819 (Tyr-567-Gly-568 in RB69 POL) into close proximity with the catalytic site (Fig. 3*A*). No adjustments were made to smooth out the joints between domains after superimposition, and only a few side chains of key residues needed to be adjusted to adopt the conformations present in the RB69 POL replicating complex (Fig. 3*A*). This simple model can easily explain the sequence activity relationship of HSV POL (Fig. 3*A*). The side chains of Asp-717, Asp-888, and carbonyl oxygen of Phe-718 (Asp-411, Asp-623, and Leu-412 in RB69 POL) are involved in metal ion coordination required for the polymerase catalysis. The ribose of the incoming nucleotide also interacts with Leu-721 and Tyr-722 and with the strictly conserved Tyr-722, providing a "steric gating" effect against incorporation of ribonucleotides (16). The positively charged side chains of Arg-785, Arg-789, and Lys-811 from the fingers domain interact with the phosphate groups of the incoming nucleotide (Fig. 3*A*) and are important for the positioning of the phosphate moiety to the 3′-OH of the primer end and for neutralizing the accumulated negative charge of the reaction intermediate (16). The side chain of Asn-815 stacks against the base of the incoming nucleotide and provides an explanation for the resistance of HSV POL N815S/T mutant to Acyclovir (5). The side chain of Tyr-818 prevents the protrusion of mismatched nascent base pairs into the DNA minor groove, ensuring the incorporation of the correct nucleotides (16). The single-stranded template would make a sharp turn at the POL active site and extend into the groove formed between the $NH_2$-terminal domain and the exonuclease domain. The DNA duplex would exit through the groove between the thumb and palm domains close to the COOH-terminal region that interacts with UL42. During rolling circle DNA replication, HSV POL could potentially interact with the viral helicase·primase complex through the pre-$NH_2$ domain to process the newly unwound single-stranded DNA template. The HSV POL accessory protein UL42 increases the processivity of the polymerase by anchoring HSV POL to the newly synthesized DNA duplex through the interactions with the COOH-terminal region.

Selective nucleoside POL inhibitors, such as Acyclovir, become active after being converted to triphosphates by viral and cellular enzymes and being incorporated into the 3′-end of the growing primer strand (3, 4). Using synthetic oligonucleotide duplex to study single dNTP incorporation, it has been shown that although Acyclovir triphosphate, mimicking a incoming dGTP substrate, can inhibit HSV POL competitively against dGTP incorporation, potent inhibition of HSV POL was observed only upon binding of the next dNTP coded by the template subsequent to the incorporation of Acyclovir monophosphate onto the 3′-end of the primer (29). Combined with the fact that the Acyclovir monophosphate-incorporated DNA duplex alone does not inhibit HSV POL strongly (29), it is fair to suggest that the dead-end complex of HSV POL with the next incoming nucleotide and the Acyclovir monophosphate-incorporated DNA duplex mimics a replicating complex. In our HSV POL replication model (Fig. 3*A*) and model of the Acyclovir monophosphate·HSV POL dead-end complex (Fig. 3*B*), the side chain of conserved residues Tyr-722 and Tyr-887 would limit modifications on the ribose for the incorporation of the inhibitor and the binding of the modified DNA duplex (3). The correctly matched base pairing of the incorporated inhibitor with the template strand, and smaller chemical moieties linked to the bases, would not be predicted to interfere with the binding of the complementary incoming nucleotide or distort the geometry of minor groove of the newly formed product DNA that would interact with the conserved KKKY (938–941) motif and the side chains of Tyr-818, Tyr-884, and Asp-886 (Fig. 3, *A* and *B*). These interactions, which involve the penultimate base pair, would normally serve the function of sensing mismatches in the newly formed DNA duplex (16). Together with the nascent base pair, these interactions are apparently sufficient to lock HSV POL into a dead-end complex, thus terminating DNA chain elongation. A large part of the specificity of these nucleoside inhibitors is derived from the specific phosphorylation of the prodrug form by viral nucleotide kinases (2), and drug resistance can arise from mutations of these viral proteins (5). Because these compounds have to be covalently incorporated, resistance mutations in the POL gene may occur at sites that modulate the kinetics of the reactions catalyzed by HSV POL. To avoid lethality, mutations that confer drug resistance against nucleoside inhibitors usually occur at sites that are not directly involved in catalysis, such as the invariant YGDTDS (884–

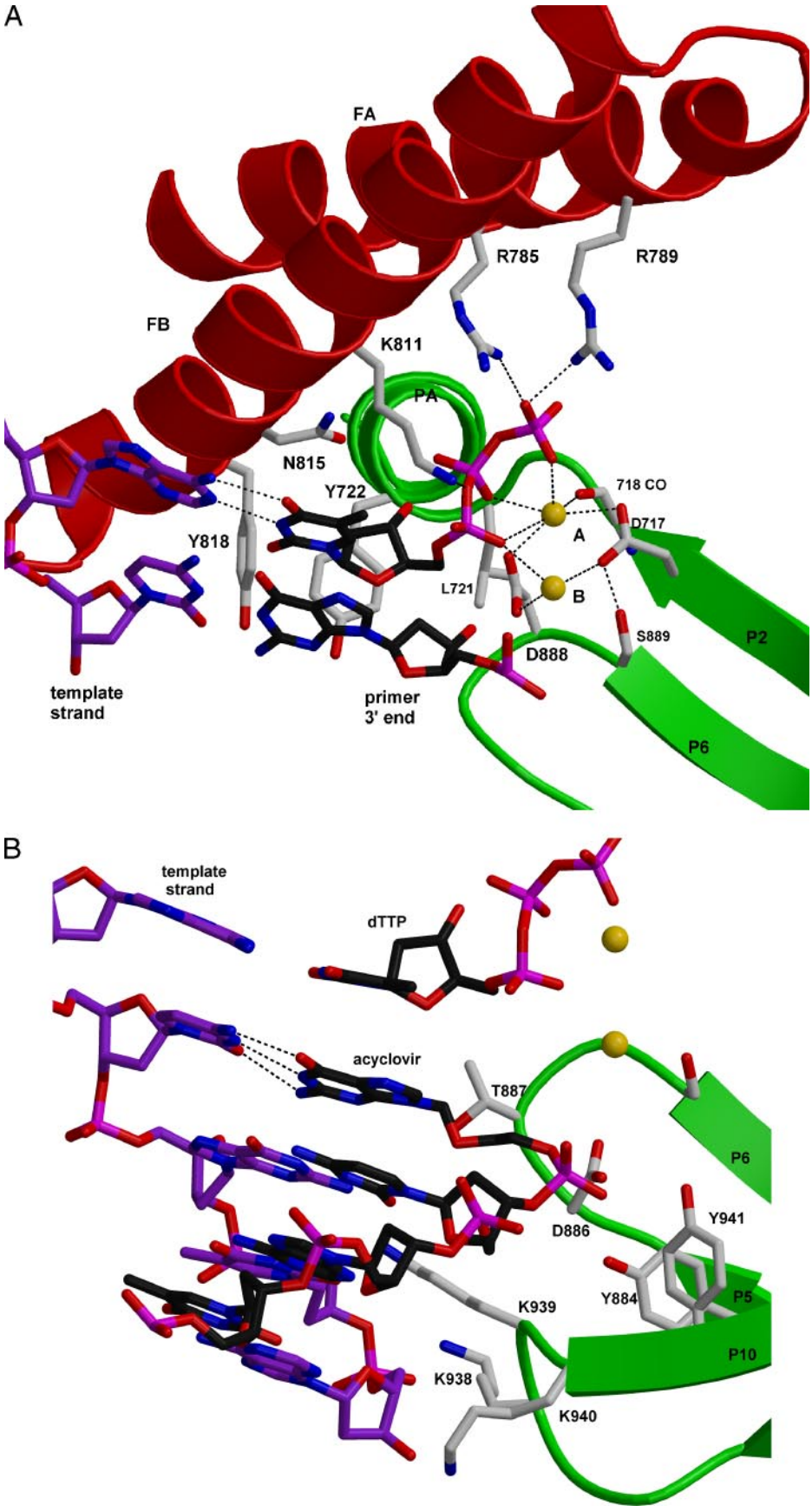


FIGURE 3. **HSV POL replicating and inhibiting model.** *A*, replicating model. The carbon atoms of HSV POL shown in *stick* are *light gray*, whereas those of primer DNA strand and dTTP are *dark gray* and those of the template are *purple*. *Black dashed lines* are shown for hydrogen bonds and ion interactions involving the incoming nucleotide and catalytic ions. *B*, model of Acyclovir·HSV POL dead-end complex. Hydrogen bonds involving Acyclovir are shown in *black dashes*. Key residues interacting with the Acyclovir-incorporated DNA, including the conserved KKKY motif (938–941), are shown. *C*, chemical structure of PNU-183792, a 4-oxo-DHQ type of herpes polymerase inhibitor. *D*, a novel inhibition mechanism of a family of broad spectrum inhibitor 4-oxo-DHQ. Residues interacting with inhibitor are *highlighted*.

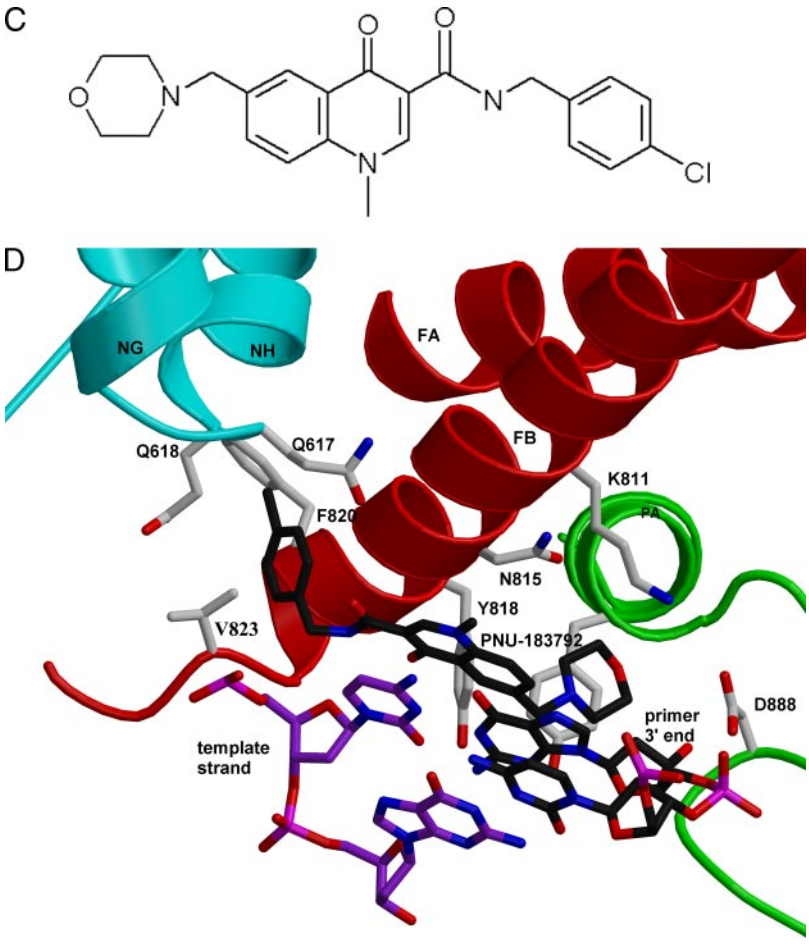


FIGURE 3—*continued*

889) sequence in region I (5). Indeed, mutations in HSV POL from the common Acyclovir-resistant virus strains cause altered $K_m$ and $K_{cat}$, but they do not directly contact with inhibitor in our model (30).

Based on models presented in Fig. 3, *A* and *B*, it is interesting to speculate why the $K_m$ for the incoming nucleotide is much higher as a substrate for the incorporation into a normal DNA duplex than the $K_d$ for its binding to a Acyclovir monophosphate-terminated one (29). Apparently, the 3′-OH of the primer strand would be in close contact with the $\alpha$ phosphate, and part of the binding energy would be utilized to overcome the repulse for the incorporation reaction (Fig. 3*A*). On the other hand, a smaller moiety and the absence of the 3′-OH group make Acyclovir monophosphate a better group to interact with the incoming nucleotide.

4-Oxo-DHQs represent an important class of non-nucleoside anti-herpes drugs and in pre-clinic trials show broad anti-HSV activity (1, 6). In contrast to nucleoside inhibitors such as Acyclovir, this class of inhibitors is not dependent on viral or cellular phosphorylation events to generate an active form and does not form covalent complexes with HSV POL. As such, the patterns of resistance against this class of agents would be predicted to be different from those of nucleoside analogs (31). The binding of a radioisotope-labeled 4-oxo-DHQ, PNU-183792 (Fig. 3*C*), to HSV POL was characterized using a near-equilibrium binding assay under conditions amenable to *in vitro* HSV POL activity assays. The results clearly showed that PNU-183792 binds only to the DNA duplex·HSV POL complex and not to the enzyme or the DNA duplex alone. The affinity of PNU-183792 toward HSV POL·DNA duplex is enhanced in the presence of $Mg^{2+}$ or $Ca^{2+}$ ions. These results explain our failure to see electron density of a 4-oxo-DHQ bound to HSV POL in either co-crystallization or soaking experiments with different compounds. Kinetic assays also showed that 4-oxo-DHQs are competitive with incoming nucleotides. These observations allowed us to propose a model for the inhibition of HSV POL by PNU-183792 (Fig. 3*D*). In our model, PNU-183792 replaces the incoming nucleotide and dislocates the template base from the active site. The aromatic moiety of PNU-183792 stacks against the base pair of the primer 3′-end and the template and also interacts with the active site residues of HSV POL (Fig. 3*D*), consistent with mutant sensitivity data of these compounds (31). The morpholine side or right side of the molecule can tolerate large modifications and locates at the phosphate binding channel. The chlorophenyl group binds to a hydrophobic pocket lined by Phe-820, Gln-617, Gln-618, and Val-823 (Fig. 3*D*). These residues are found in mutant virus strains that have dramatically decreased binding affinity for 4-oxo-DHQ (31). The location of the chlorophenyl group also explains the tight structure-activity relationship observed on 4-oxo-DHQs (34).

## DISCUSSION

Analysis of HSV POL suggests the existence of a putative viral primase/helicase-interacting domain and the location of a putative RNA binding domain. If confirmed, they enrich our understanding of how herpes viruses replicate and also provide additional pathways to develop anti-herpes drugs. The replication model of HSV POL presented here also gives clues on viral replication. The detailed dead-end complex model of HSV POL with Acyclovir provides an explanation at the molecular level of drug resistance and a basis for improving these existing drugs. Finally, the novel inhibition mechanism of the 4-oxo-DHQs

may provide a strategic insight for the development of anti-herpetic drugs and the discovery of drugs against other viruses.

*Acknowledgments—We thank Tim Benson, Barry Finzel, and Bill Watts for help with data collection and discussion.*

## REFERENCES


1. Coen, D. M., and Schaffer, P. A. (2003) *Nat. Rev.* **2,** 278–288
2. Elion, G. B. (1989) *Science* **244,** 241–247
3. De Clercq, E. (2001) *J. Clin. Virol.* **22,** 73–89
4. Bacon, T. H., Levin, M. J., Leary, J. J., Sarisky, R. T., Sutton, D. (2003) *Clin. Microbiol. Rev.* **16,** 114–128
5. Gilbert, C., Bestman-Smith, J., and Boivin, G. (2002) *Drug Resistance Update* **5,** 88–114
6. Wathen, M. W. (2002) *Rev. Med. Virol.* **12,** 167–178
7. Lehman, I. R., and Boehmer, P. E. (1999) *J. Biol. Chem.* **274,** 28059–28062
8. Knopf, K. W. (1979) *Eur. J. Biochem.* **98,** 231–244
9. Crute, J. J., and Lehman, I. R. (1989) *J. Biol. Chem.* **264,** 19266–19270
10. Digard, P., Bebrin, W. R., Weisshart, K., and Coen, D. M. (1993) *J. Virol.* **67,** 398–406
11. Zuccola, H. J., Filman, D. J., Coen, D. M., and Hogle, J. M. (2000) *Mol. Cell* **5,** 267–278
12. Rodriguez, A. C., Park, H. W., Mao, C., and Beese, L. S. (2000) *J. Mol. Biol.* **299,** 447–462
13. Zhao, Y., Jeruzalmi, D., Moarefi, I., Leighton, L., Lasken, R., and Kuriyan, J. (1999) *Structure* **7,** 1189–1199
14. Wang, J., Sattar, A., Wang, C. C., Karam, J. D., Konigsberg, W. H., and Steitz, T. A. (1997) *Cell* **89,** 1087–1099
15. Shamoo, Y., and Steitz, T. A. (1999) *Cell* **99,** 155–166
16. Franklin, M., Wang, J., and Steitz, T. A. (2001) *Cell* **105,** 657–667
17. Bellizzi, J. J., III, Widom, J., Kemp, C., Lu, J. Y., Das, A. K., Hofmann, S. L., and Clardy, J. (2000) *Proc. Natl. Acad. Sci. U. S. A.* **97,** 4573–4578
18. Otwinowski, Z., and Minor, W. (1997) in *Macromolecular Crystallography* (Carter, J. C. W., and Sweet, R. M., eds) pp. 307–326, Academic Press, New York
19. Collaborative Computing Project 4 (1994) *Acta Crystallogr. Sect. D Biol. Crystallogr.* **50,** 760–763
20. Uson, I., and Sheldrick, G. M. (1999) *Curr. Opin. Struct. Biol.* **9,** 643–648
21. Abrahams, J. P. (1996) *Acta Crystallogr. Sect. D Biol. Crystallogr.* **52,** 30–42
22. Vagin, A., and Teplyakov, A. (1997) *J. Appl. Crystallogr.* **30,** 1022–1025
23. Jones, T. A., Zou, J.-Y., Cowan, S. W., and Kjeldgaard, M. (1991) *Acta Crystallogr. Sect. A*, **47,** 110–119
24. Brunger, A. T. (1992) XPLOR Version 3.1., Yale University Press, New Haven, CT
25. Murshudov, G. N., Vagin, A. A., and Dodson, E. J. (1997) *Acta Cryst. Sect. D Biol. Crystallogr.* **53,** 240–255
26. Kleywegt, G. J., Zou, J. Y., Kjedgaard, M., and Jones, T. A. (2001) in *International Tables for Crystallography* (Rossmann, M. G., and Arnold, E., eds) Vol. F, pp. 353–356, Kluwer Academic Publishers, Dordrecht, The Netherlands
27. Hwang, Y. T., Liu, B. Y., Hong, C. Y., Shillitoe, E. J., and Hwang, C. B. C. (1999) *J. Virol.* **73,** 5326–5332
28. Burd, C. G., and Dreyfuss, G. (1994) *Science* **26,** 615–621
29. Reardon, J. E., and Spector, T. (1989) *J. Biol. Chem.* **264,** 7405–7411
30. Huang, L., Ishi, K. K., Zuccola, H., Gehring, A. M., Hwang C. B. C., Hogle, J., and Coen, D. M. (1999) *Proc. Natl. Acad. Sci. U. S. A.* **96,** 447–452
31. Thomsen, D. R., Oien, N. L., Hopkins, T. A., Knechtel, M. L., Brideau, R. J., Wathen, M. W., and Homa, F. L. (2003) *J. Virol.* **77,** 1868–1876
32. Kraulis, P. J. (1991) *J. Appl. Crystallogr.* **24,** 946–950
33. DeLano, W. L. (2002). The PyMOL Molecular Graphics System, DeLano Scientific, San Carlos, CA
34. Schnute, M. E., Cudahy, M. M., Brideau, R. J., Homa, F. L., Hopkins, T. A., Knechtel, M. L., Oien, N. L., Pitts, T. W., Poorman, R. A., Wathen, M. W., Wieber, J. L. (2005) *J Med. Chem.* **48,** 5794–5804

**Crystal Structure of the Herpes Simplex Virus 1 DNA Polymerase**

Shenping Liu, John D. Knafels, Jeanne S. Chang, Gregory A. Waszak, Eric T. Baldwin, Martin R. Deibel, Jr., Darrell R. Thomsen, Fred L. Homa, Peter A. Wells, Monica C. Tory, Roger A. Poorman, Hua Gao, Xiayang Qiu and Andrew P. Seddon

*J. Biol. Chem. 2006, 281:18193-18200.*
*doi: 10.1074/jbc.M602414200 originally published online April 24, 2006*

---